

**Measurement of the total hadronic cross section
in e^+e^- annihilation at $\sqrt{s} = 29 \text{ GeV}^*$**

C. von Zanthier,⁽²⁾ W. de Boer,^{(4)(a)} G. Grindhammer,^{(4)(b)} J. Hylen,⁽⁶⁾
 B. Harral,⁽⁶⁾ C. Hearty,^(l) L. Labarga,^{(2)(c)} J. Matthews,⁽ⁱ⁾ M. Schaad,^{(1)(d)}
 G. Abrams,⁽¹⁾ C. E. Adolphsen,⁽²⁾ C. Akerlof,⁽⁷⁾ J. P. Alexander,^{(4)(l)}
 M. Alvarez,^{(9)(e)} A. R. Baden,^{(1)(o)} J. Ballam,⁽⁴⁾ B. C. Barish,⁽⁵⁾ T. Barklow,⁽⁴⁾
 B. A. Barnett,⁽⁶⁾ J. Bartelt,⁽⁴⁾⁽⁺⁾ D. Blockus,⁽³⁾ G. Bonvicini,^{(7)(j)}
 A. Boyarski,⁽⁴⁾ J. Boyer,⁽¹⁾ B. Brabson,⁽³⁾ A. Breakstone,⁽⁸⁾ J. M. Brom,^{(3)(m)}
 F. Bulos,⁽⁴⁾ P. R. Burchat,⁽²⁾ D. L. Burke,⁽⁴⁾ F. Butler,^{(1)(s)} F. Calvino,⁽⁹⁾⁽ⁱ⁾
 R. J. Cence,⁽⁸⁾ J. Chapman,⁽⁷⁾ D. Cords,⁽⁴⁾ D. P. Coupal,⁽⁴⁾ H. C. DeStaebler,⁽⁴⁾
 D. E. Dorfan,⁽²⁾ J. M. Dorfan,⁽⁴⁾ P. S. Drell,^{(1)(l)} G. J. Feldman,⁽⁴⁾
 E. Fernandez,^{(9)(e)} R. C. Field,⁽⁴⁾ W. T. Ford,⁽⁹⁾ C. Fordham,⁽⁴⁾ R. Frey,^{(7)(t)}
 D. Fujino,⁽⁴⁾ K. K. Gan,⁽⁴⁾ G. Gidal,⁽¹⁾ T. Glanzman,⁽⁴⁾ G. Goldhaber,⁽¹⁾
 A. Green,^{(4)(r)} P. Grosse-Wiesmann,^{(4)(j)} J. Haggerty,^{(1)(f)} G. Hanson,⁽³⁾
 R. Harr,⁽¹⁾ F. A. Harris,⁽⁸⁾ C. M. Hawkes,^{(5)(j)} K. Hayes,⁽⁴⁾ D. Herrup,⁽¹⁾⁽ⁿ⁾
 C. A. Heusch,⁽²⁾ T. Himel,⁽⁴⁾ M. Hoenk,⁽⁵⁾ D. Hutchinson,⁽⁴⁾ W. R. Innes,⁽⁴⁾
 M. Jaffre,^{(1)(p)} J. A. Jaros,⁽⁴⁾ I. Juricic,^{(1)(k)} J. A. Kadyk,⁽¹⁾ D. Karlen,^{(4)(h)}
 J. Kent,⁽²⁾ S. R. Klein,^{(4)(g)} W. Koska,⁽⁷⁾⁽ⁿ⁾ W. Kozanecki,⁽⁴⁾ A. J. Lankford,⁽⁴⁾
 R. R. Larsen,⁽⁴⁾ M. E. Levi,⁽¹⁾ Z. Li,⁽⁵⁾ A. M. Litke,⁽²⁾ V. Lüth,⁽⁴⁾ D. I. Meyer,⁽⁷⁾
 B. D. Milliken,⁽⁵⁾ K. C. Moffeit,⁽⁴⁾ L. Müller,^{(4)(q)} J. Nash,⁽⁴⁾ M. E. Nelson,⁽ⁱ⁾
 D. Nitz,⁽⁷⁾ H. Ogren,⁽³⁾ K. F. O'Shaughnessy,⁽⁴⁾ S. I. Parker,⁽⁸⁾ C. Peck,⁽⁵⁾
 M. L. Perl,⁽⁴⁾ A. Petersen,^{(4)(v)} M. Petradza,⁽⁴⁾ F. C. Porter,⁽⁵⁾ P. Rankin,⁽⁹⁾
 K. Riles,^{(4)(z)} D. R. Rust,⁽³⁾ H. F. W. Sadrozinski,⁽²⁾ T. L. Schalk,⁽²⁾
 W. B. Schmidke,⁽¹⁾ A. S. Schwarz,^{(2)(b)} A. Seiden,⁽²⁾ J. G. Smith,⁽⁹⁾ A. Snyder,⁽³⁾
 E. Soderstrom,⁽⁵⁾ D. P. Stoker,⁽⁶⁾ R. Stroynowski,⁽⁵⁾ R. Thun,⁽⁷⁾ G. H. Trilling,⁽¹⁾
 R. Tschirhart,^{(7)(u)} R. Van Kooten,⁽⁴⁾ H. Veltman,^{(7)(y)} P. Voruganti,^{(4)(x)}
 S. R. Wagner,⁽⁴⁾ P. Weber,⁽⁹⁾ A. J. Weinstein,⁽⁵⁾ A. J. Weir,⁽⁵⁾ S. Weisz,^{(2)(j)}
 S. L. White,^{(9)(w)} E. Wicklund,⁽⁵⁾ D. R. Wood,^{(1)(j)} and D. Y. Wu⁽⁵⁾

The MARK II Collaboration

Submitted to Physical Review D.

* Work supported in part by Department of Energy contracts DE-AC03-76SF00515 (SLAC), DE-AC03-81ER40050 (CIT), DE-AM03-76SF00010 (UCSC), DE-AC02-86ER40253 (Colorado), DE-AC03-83ER40103 (Hawaii), DE-AC02-84ER40125 (Indiana), DE-AC03-76SF00098 (LBL), and DE-AC02-84ER40125 (Michigan), and by the National Science Foundation (Johns Hopkins).

- (1) *Lawrence Berkeley Laboratory and Department of Physics,
University of California, Berkeley, California 94 720*
- (2) *University of California, Santa Cruz, California 95064*
- (3) *Indiana University, Bloomington, Indiana 47405*
- (4) *Stanford Linear Accelerator Center, Stanford University,
Stanford, California 94309*
- (5) *California Institute of Technology, Pasadena, California 91125*
- (6) *Johns Hopkins University, Baltimore, Maryland 21218*
- (7) *University of Michigan, Ann Arbor, Michigan 48109*
- (8) *University of Hawaii, Honolulu, Hawaii 96822*
- (9) *University of Colorado, Boulder, Colorado 80309*

- (a) Present address: Universitat Karlsruhe, D-7500 Karlsruhe, F. R. Germany
- (b) Present address: Max-Planck Institut, München, F. R. Germany
- (c) Present address: Universidad Autónoma de Madrid, Canto Blanco, Madrid, Spain
- (d) Present address: Elektrowatt Ingenieurunternehmung AG, CH-8034 Zurich, Switzerland
- (e) Present address: Universidad Autónoma de Barcelona, Bellaterra, Spain
- (f) Present address: Brookhaven National Laboratory, Upton, NY 11973
- (g) Present address: Boston University, Boston, MA 02215
- (h) Present address: Carleton University, Ottawa, Ontario, Canada, K1S 5B6
- (i) Present address: Universitat Politecnica de Catalunya, ETSEIB-DEN Barcelona, Spain
- (j) Present address: CERN, CH-1211, Genève 23, Switzerland
- (k) Present address: Columbia University, New York, NY 10027
- (l) Present address: Cornell University, Ithaca, NY 14853
- (m) Present address: Centre de Recherches Nucleaires, F-67037 Strasbourg, France
- (n) Present address: Fermi National Laboratory, Batavia, IL 60510
- (o) Present address: Harvard University, Cambridge, MA 02138
- (p) Present address: Laboratoire de l'Accélérateur Linéaire, F-91405 Orsay, France
- (q) Present address: Lab. für Hochenergie Physik Bern, CH-3012 Bern, Switzerland
- (r) Present address: O'Conner and Associates, Chicago, IL 60604
- (s) Present address: University of Oklahoma, Norman, OK 73019
- (t) Present address: University of Oregon, Eugene, OR 97403
- (u) Present address: Princeton University, Physics Department, Princeton, NJ 08544
- (v) Present address: SCS, Hamburg, F. R. Germany
- (w) Present address: University of Tennessee, Knoxville, TN 37996
- (x) Present address: University of Toronto, Toronto, Ontario, Canada
- (y) Present address: University of California, Berkeley, CA 94720
- (z) Present address: University of California, Riverside, CA 92521
- (+) Present address: Vanderbilt University, Nashville, TN 37235

A precise measurement of the ratio R of the total cross section $e^+e^- \rightarrow \mathbf{hadrons}$ to the point like cross section $e^+e^- \rightarrow \mu^+\mu^-$ at a center-of-mass energy of 29.0 GeV is presented. The data were taken with the upgraded MARK II detector at PEP. The result, is $R = 3.92 \pm 0.05 \pm 0.09$. The luminosity has been determined with three independent luminosity monitors measuring Bhabha scattering at different angular intervals. Recent calculations of higher-order QED radiative corrections are used to estimate the systematic error due to missing higher-order radiative corrections in the Monte Carlo event generators.

1. INTRODUCTION

Since early on in e^+e^- physics there has been an effort to precisely measure R , the ratio of the hadronic cross section $\sigma_h(e^+e^- \rightarrow \mathbf{hadrons})$ to the pointlike cross section $\sigma_\mu^0(e^+e^- \rightarrow \gamma \rightarrow \mu^+\mu^-)$, at all accessible center-of-mass energies. R has been measured at the storage rings ADONE,¹ SPEAR,² CESR,³ and DORIS⁴ at energies below 11 GeV, at 29 GeV with PEP,⁵ up to 47 GeV with PETRA⁶ and between 50 and 61.4 GeV at KEK.⁷ All measurements of R so far give impressive support to many aspects of the Standard Model. For example, the measurements give evidence for the fractional electric charge of the quarks and the three colors of the strong force. In addition, the strong coupling constant α_s and the electroweak mixing angle have been determined from fitting R values over a large range of center-of-mass energies.^{8,9}

In the Standard Model, hadron production in e^+e^- collisions at center-of-mass energies well above quark-mass thresholds proceeds through the formation of a virtual photon or Z^0 boson, which “decays” into a quark-antiquark pair. The free quarks dress themselves into hadrons that reach the detector in a jetlike formation. In this

model R is:¹⁰

$$\begin{aligned}
\mathbf{R}(s) &\equiv \frac{\sigma_h^0[e^+e^- \rightarrow \gamma, Z^0 \rightarrow \text{hadrons}]}{\sigma_\mu^0[e^+e^- \rightarrow \gamma \rightarrow \mu^+\mu^-]} \\
&= N_c \cdot \sum_q \left\{ Q_q^2 - \frac{\sqrt{2}G_F}{16\pi\alpha} Q_q v_e v_q \frac{2s}{(s/m_Z^2 - 1) + ((\Gamma_Z^2/(s - m_Z^2)))} \right. \\
&\quad \left. + \frac{G_F^2}{128\pi^2\alpha} (v_q^2 + a_q^2)(v_e^2 + a_e^2) \frac{s^2}{(s/m_Z^2 - 1)^2 + (\Gamma_Z^2/m_Z^2)} \right\} \\
&\quad \times \left(1 + \frac{\alpha_s(s)}{\pi} + C_2 \left(\frac{\alpha_s(s)}{\pi} \right)^2 + C_3 \left(\frac{\alpha_s(s)}{\pi} \right)^3 + \dots \right) , \tag{1}
\end{aligned}$$

where the sum runs over all quark flavors. N_c is the number of quark colors, i.e., $N_c = 3$. Q_q is the electric charge of the quarks, G_F is the Fermi weak constant, α is the fine structure constant, α_s the running strong coupling constant, and m_Z and Γ_Z are the mass and the width of the Z^0 boson; $v_e, v_q, a,$ and a_q are the vector and axial vector coupling constants which are given in the Standard Model:

$$v_e = -1 + 4 \sin^2 \theta_W , \quad a_e = -1 \tag{2}$$

$$v_u = v_c = 1 - \frac{8}{3} \sin^2 \theta_W , \quad a_u = a_c = 1 \tag{3}$$

$$v_d = v_s = v_b = -1 + \frac{4}{3} \sin^2 \theta_W , \quad a_d = a_s = a_b = -1 . \tag{4}$$

The power series in α_s in Eq. (1) accounts for gluon emission by the two final state quarks and contributes approximately 6% to the cross section. The coefficients C_2 and C_3 are renormalization scheme dependent. In the $\overline{\text{MS}}$ scheme they have been calculated to be¹¹ $C_2 = 1.986 - 0.115N_f$ and recently $C_3 = 64.71$.¹² The superscript in σ^0 indicates that all radiative QED corrections are excluded from the cross sections; i.e., $\sigma_\mu^0 = 4\pi\alpha^2/3s$ and the measured hadronic cross section has to be corrected for

higher-order QED processes. Expressions due to quark mass effects are omitted in Eq. (1) since their contribution to R at $\sqrt{s} = 29$ GeV is negligible. The electroweak contribution to R at this energy is 0.3% for $\sin^2 \theta_W = 0.23$.

Experimentally, R is measured by normalizing the number of observed hadronic events to the luminosity, as determined by the event counts of a well understood process. We use Bhabha events to determine the luminosity and obtain:

$$R = \frac{N_h}{N_b} \frac{\epsilon_b}{\epsilon_h} \frac{(1 + \delta_b)}{(1 + \delta_h)} \frac{\sigma_b^0}{\sigma_\mu^0}, \quad (5)$$

where $N_h(N_b)$ is the number hadronic (Bhabha) events found after selection cuts and background subtraction, $\epsilon_h(\epsilon_b)$ is the hadron (Bhabha) detection efficiency determined from Monte Carlo simulations, $\delta_h(\delta_b)$ is the correction to the Born level hadronic (Bhabha) cross section due to higher-order QED processes, and σ_b^0 is the Born level Bhabha cross section.

In this paper we present a precise measurement of R with data taken using the upgraded MARK II detector at the SLAC e^+e^- storage ring PEP at a center-of-mass energy of 29 GeV. Important features of this analysis include: separate determination of the luminosity by three different detector subsystems; use of an improved LUND Monte Carlo program, which provides an excellent description of the fragmentation process for the determination of the hadronic efficiency; and the use of recently produced Monte Carlo programs, which include QED effects beyond $O(\alpha^3)$ and allow for estimates of systematic errors due to higher-order radiative processes.

2. THE UPGRADED MARK II DETECTOR

The upgrade of the MARK II detector as it was previously used at SPEAR and PEP consists of several added or changed detector components. These changes were

motivated by the demands for the upcoming MARK II runs at the Stanford Linear Collider (SLC). The changes relevant for our analysis consist of a new Drift Chamber (DC), a higher magnetic field, a new End Cap Calorimeter (ECC), and an improved trigger. A Small Angle Tagger (SAT) and a Trigger Chamber (TC) were added for data taking at PEP but not for the SLC. With the exception of the SAT (see Appendix A), details of the upgrade are described elsewhere.^{13,14} We will therefore only briefly mention those detector components that are essential for this analysis.

Charged particles from an event pass from the interaction point through the aluminum beampipe to the TC and DC, where they are tracked. The TC [Ref. 14] was built for the upgraded MARK II at PEP only. It consists of a concentric, six-layer array of single-wire drift chamber cells aligned coaxially with the beampipe. The radius of the inner layer of the TC is 9.5 cm; the outer layer radius is 14.8 cm. With an active length of 75 cm for each wire, the TC fully covers all tracks with a polar angle of $|\cos \theta| < 0.93$ with respect to the electron beam direction. The TC is used for event triggering purposes and improves the tracking resolution of the DC.

The DC [Ref. 15] is designed to handle the high multiplicity events and high energy tracks that the MARK II would encounter at the SLC. Its track separation and momentum resolution at PEP energies is therefore excellent. The DC design is based on the jet-chamber configuration¹⁶; it is structured in drift cells, each containing 6 sense wires, which are arranged in 12 concentric layers around the TC. The outer radius of the DC is 151.9 cm and the active length is 230 cm. DC tracking has high efficiency down to $|\cos \theta| < 0.85$. The typical momentum resolution at the specified magnetic field of 4.5 kG is $\sigma_p/p^2 = 0.3\% \text{ GeV}^{-1}$ without a vertex constraint. The material in the direction perpendicular to the beampipe over all layers of the TC and DC together corresponds to an average thickness of 0.038 radiation lengths; the

thickness of the beampipe by itself is 0.0143 radiation lengths.

The DC is surrounded by a Time-of-Flight (TOF) scintillator counter system covering the polar angle region $|\cos \theta| < 0.70$. Outside the TOF is the magnetic coil, which provides a homogeneous magnetic field of 4.5 kG in the z -direction. The thickness of the coil corresponds to 1.3 radiation lengths.

Around the coil is the Liquid Argon Calorimeter (LAC),¹⁷ a lead liquid-argon sampling device, which was also used for the earlier runs at SPEAR and PEP. The LAC consists of eight rectangular modules, each having a volume of $1.5 \times 3.8 \times 0.21 \text{ m}^3$ that cover the polar angle $|\cos \theta| < 0.68$. The energy resolution for Bhabha tracks is $\sigma/E = 4.6\%$. The spatial resolution is 3 mrad in ϕ and 8 mm in z . The thickness of the LAC corresponds to 16 radiation lengths.

The new End Cap Calorimeter (ECC) increases the calorimetric coverage to 86% of the total solid angle. It is made of a lead-proportional tube structure, which amounts to a thickness of 18 radiation lengths at perpendicular incidence. The energy resolution is measured to be $22\%/\sqrt{E}$ (E in GeV). The position resolution is 0.27 cm in the x and in y direction. The distance in z from the first layer to the interaction point is 137 cm.

The MARK II trigger uses calorimetric and charged track information. Charged tracks are identified with hardware curvature modules. Showers in the calorimeters are considered if the deposited energy in one of the ten modules (eight LAC modules and two ECC modules) passes a threshold of 1 to 2 GeV. The trigger logic requires either: (a) two well identified charged tracks with associated TOF hits, (b) one well identified charged track with TOF hit and one calorimetric module hit, or (c) two energy depositions above threshold in opposite calorimeter modules. For the ECC modules one of the hits has to deposit more than 7 to 9 GeV.

3. HADRONIC EVENT ANALYSIS

3.1 Event Selection

For the selection of hadronic events, we use drift chamber information for charged tracks and calorimeter information for neutral tracks.

Charged tracks have to pass the following cuts:

- (1) transverse momentum $p_{xy} > 100$ MeV;
- (2) angle with respect to the beam direction $|\cos \theta| < 0.825$;
- (3) distance of closest approach to the event vertex $|r_{tr} - r_v| < 5$ cm, $|z_{tr} - z_v| < 7$ cm; and
- (4) total momentum $p < (E_{cm})/2 (1 + 0.015E_{cm})$.

Cut (1) rejects spiral tracks, Cut (2) defines the high quality DC fiducial volume, Cut (3) mainly rejects tracks from cosmic rays and beam-gas events' and Cut (4) removes poorly reconstructed tracks with unphysical momentum. Only 0.5% of the final event sample had such a track removed.

Neutral tracks have to pass the cuts:

- (1) shower energy $E_{sh} > 250$ MeV;
- (2) no charged track within 30 cm of the shower at the front face of the calorimeter; and
- (3) angle with respect to the beam direction $|\cos(\theta)| < 0.825$.

Cut (1) ensures a high shower reconstruction efficiency, Cut (2) keeps neutral showers separated from from charged track showers. The value in Cut (3) is taken to match the charged particle acceptance.

Hadronic events are selected by applying the following requirements:

- (1) number of charged tracks $N_{ch} > 4$;
- (2) charged energy $E_{ch} > 0.26 E_{cm}$;
- (3) total visible energy $E_{vis} > 0.4 E_{cm}$;
- (4) momentum balance: $p_T \equiv \sqrt{(\sum p_{x_i})^2 + (\sum p_{y_i})^2} < 10 \text{ GeV}$ and $|\sum p_{z_i}| < 10 \text{ GeV}$, where the sums run over charged and neutral tracks;
- (5) charge balance $|\sum q_i| < 5$, where q_i is the charge of the i^{th} track; and
- (6) the z coordinate of the event vertex to be within 6 cm of the average measured interaction point, $|Z_v| < 6 \text{ cm}$.

The charged multiplicity cut rejects Bhabha, $\mu^+\mu^-$, $\tau^+\tau^-$ and two photon events. The charged and visible energy cuts reject mainly two photon and beam gas events. The balanced momentum requirement cuts two photon, beam gas and $\tau^+\tau^-$ events. It also removes events with a very hard initial state photon escaping down the beampipe. Cuts (5) and (6) reject beam gas events.

3.2 Hadronic Efficiency

In order to calculate the efficiency ϵ_h for these cuts we have used the Lund Monte Carlo version 6.3.¹⁸ This Monte Carlo uses the $O(\alpha^3) e^+e^- \rightarrow q\bar{q}(\gamma)$ QED generator from Berends, Kleiss and Jadach,¹⁹ followed by the parton shower evolution generator which uses coherent branching and $O(\alpha_s)$ matrix element,²⁰ and the Lund string hadronization which uses the Lund string fragmentation function for all flavors. The set of values used for the fragmentation parameters is described in a previous paper.²¹

Figure (1) shows a comparison between data and the hadronic event Monte Carlo. The distributions plotted are: (a) charged multiplicity, (b) charged energy, (c) cosine of the angle between the thrust axis and the beam direction, and (d) thrust.

Only the events surviving all the cuts have been used for the plots. The overall agreement is good. The differences observed at low N_{ch} and low E_{ch} are due to background in the data and will be discussed in the next section.

The number of events passing the selection cuts and their estimated efficiency ϵ_h are shown in Table I. These values are obtained from the Monte Carlo with the maximum initial state photon energy $k_{max} \equiv (E_\gamma^{max})/E_{beam}$ set to the Lund default value $k_{max} = 0.99$. We find that the product $\epsilon_h \cdot (1 + \delta_h)$ is equal to 0.843 ± 0.003 , where the error is statistical only.

3.3 Hadronic Backgrounds and Systematic Errors

The following sources of background contributing to our final hadronic sample have been investigated:

1. Vertices from beam gas events tend to be homogeneously distributed in the beampipe along the beam direction Z . Only five events with $6 \text{ cm} < |Z_v| < 30 \text{ cm}$ are rejected by the final $|Z_v|$ vertex cut. In addition, a visual scan of a significant fraction of the data shows no beam gas event candidate. Hence, the number of beam gas events in the hadronic sample is negligible.
2. The $e^+e^- \rightarrow e^+e^-q\bar{q}$ background is described by two different models:
 - (a) One is the Vector Dominance Model (VDM)-like process, which tends to have low E_{vis} with the electron and positron going undetected into the beampipe. This background is therefore strongly suppressed by E_{ch} and E_{vis} cuts. Since the uncertainty in the cross section for this process is large, we made a crosscheck by comparing the shape of the low energy tail of the E_{ch} distributions before making the energy cut of the data with the VDM Monte Carlo events. An extrapolation of the Monte Carlo data tail

to higher E_{ch} predicts a small two-photon contamination. We estimate the VDM-like two-photon background to be $0.3\% \pm 0.3\%$.

(b) The other process is well described by the QED-like model. We used the complete lowest-order Monte Carlo calculation²² and obtained a contamination of $0.7\% \pm 0.3\%$.

3. Background due to pair production of $\tau^+\tau^-$ has been estimated by Monte Carlo simulations. We find a 0.9% background with an uncertainty of 0.4%. We have checked the result by studying the behavior of the hadronic sample when extra cuts to eliminate τ events are applied. Another check has been the visual scan of low charged multiplicity events.

4. The contribution of high multiplicity Bhabha events to the hadronic sample has been investigated by scanning low charged multiplicity events. The contribution was estimated to be 0.5% with an uncertainty of 0.3%.

We studied the stability of the ratio of the number of hadrons with the detection efficiency, N_h/ϵ_h , against variations of track and event selection cuts:

- Variations of the track selection cuts:
 - o For $|\cos \theta| > 0.825$ the track reconstruction efficiency for multihadronic events decreases rapidly, a fact which is not very well simulated by the Monte Carlo. Varying the $|\cos \theta|$ cut from 0.5 to 0.9 we obtain an uncertainty of 1.1%.
 - o The same kind of variation in the θ cut has been carried out for the reconstructed showers in the calorimeter. No significant variation has been found.
 - o Reasonable variations of the cut on the track's closest distance to the reconstructed vertex gives an uncertainty in N_h/ϵ_h of 0.2%.

- Variations of the hadronic selection cuts:
 - We have increased the minimum number of reconstructed charged tracks for the event to be selected, and find uncertainties of 0.6%.
 - Variations of the E_{ch} and E_{vis} cuts produce changes in N_h/ϵ_h of 0.9% and 0.4%, respectively.
 - Uncertainties from the balanced momentum cut are estimated to be 0.2%.
 - Another uncertainty is the hadronization Monte Carlo used for the estimation of ϵ_h . Using the Webber Monte Carlo tuned to the MARK II data²¹ we find a variation of 0.4%, compatible with our statistical error on the number of Monte Carlo events generated.

Figure (2) shows the variation of N_h/ϵ_h with the particular values used for some of the cuts: (a) charged multiplicity, (b) charged energy, (c) fiducial volume for tracks, and (d) visible energy. The estimated backgrounds in each of the bins have not been subtracted.

Table II summarizes the background contributions, the systematic error estimations, and our final hadronic sample.

4. LUMINOSITY MEASUREMENT

The luminosity was measured by counting Bhabha events. We looked at Bhabha tracks in three separate ranges of θ using different elements of the detector. We therefore obtain three largely independent luminosity measurements. The first luminosity measurement is done with wide-angle Bhabha tracks going into the LAC ($|\cos \theta| < \mathbf{0.65}$). The second measurement uses the forward scattered Bhabha tracks going into the ECC ($0.74 < |\cos \theta| < 0.86$). The third measurement is done with the SAT ($0.9987 < |\cos \theta| < 0.9998$).

4.1 Liquid Argon Calorimeter Bhabha Luminosity Measurement

Measuring the luminosity with wide-angle Bhabha events has two advantages: (i) the tracks lie well within the acceptance of the DC and LAC, yielding redundant, track and trigger information; and (ii) the fiducial volume cut is less critical due to the less steeply rising Bhabha cross section in θ .

The selection criteria for Bhabha events are:

1. ~~Raw~~ Fiducial Volume Cut: The event must have at least two LAC showers within the polar angle region $|\cos \theta| < 0.65$; the shower also must be away from the center of the eight LAC barrel cracks by at least ± 0.06 rad in ϕ .
2. Energy Cut 1: A cone (Cone 1) centered around the shower with the highest LAC energy, with opening angles $\Delta\phi = \Delta\theta = 0.05$ rad, is searched for additional showers. The LAC-energy sum of all showers within this cone has to be larger than 5 GeV. The concept of the cone is introduced to include Bhabha events where the electron or positron track has lost energy to a hard bremsstrahlung or a final state photon. Of all Bhabha track cones, 0.9% contain more than one LAC shower, which is only poorly simulated in the Monte Carlo data.
3. Energy Cut 2: The area on the opposite side of Cone 1 within an acollinearity angle of 0.4 rad is searched for LAC showers. The shower with the highest energy is used as the center for another cone (Cone 2) of the same size as Cone 1. The LAC energy sum of all showers within this cone has to be larger than 5 GeV.
4. Final Energy Cut: To reject $\tau^+\tau^-$ background one of the two cone energies is required to be larger than 10 GeV. This cut reduces the data sample by 0.3% with no loss in detection efficiency.
5. Charged Track Cut: There must be only one charged track in the angular region within 0.4 rad around one of the two cone center axes. The same angular

region around the cone on the opposite side may have from zero to three charged tracks. This cut rejects background coming from $e^+e^- \rightarrow \gamma\gamma$. The cut reduces the data sample by 10.6% while leaving the efficiency unchanged.

6. Fine/Gross Fiducial Volume Cut: The center shower of one of the cones must lie within the fine fiducial volume $|\cos \theta_2| < 0.60$; the center shower of the other cone is allowed to be within the gross fiducial volume $|\cos \theta_1| < 0.63$. This fine/gross cut is introduced to avoid an implicit small-angle acollinearity cut for opposite Bhabha tracks close to the fiducial volume edge. Whenever a shower is linked to a charged track, the angle is measured with the DC because of its better angular resolution.

A total of 13295 events pass these cuts. To get an estimate for the systematic error due to these cuts we vary the cut parameters. The cone energy cuts were varied from 3 to 8 GeV, with the final cone energy cut was varied from 8 to 11 GeV; these changes, affected the luminosity value by less than $\pm 0.8\%$. The acollinearity angle between the two cone axes was varied from 0.3 to 0.5 rad which changed the luminosity value by less than $\pm 0.3\%$. Moving $\cos \theta_1$ and independently $\cos \theta_2$ from 0.63 to 0.54 changes \mathcal{L} by $\pm 0.4\%$.

The main background sources in the Bhabha sample are the processes $e^+e^- \rightarrow \tau^+\tau^-$, $e^+e^- \rightarrow \gamma\gamma$, and $e^+e^- \rightarrow e^+e^-e^+e^-$. We used Monte Carlo simulations to estimate these backgrounds. Both the $\tau^+\tau^-$ and $e^+e^-e^+e^-$ contamination in the Bhabha sample are found to be less than 0.1%; the $\gamma\gamma$ contamination is 1.1% with an estimated uncertainty of 0.5%.

The trigger efficiency ϵ_{tr} is measured using the redundancy between the neutral and charged trigger. It is found to be 0.998 ± 0.001 .

The accepted cross section of $\sigma_b \epsilon_b = 611.4 \text{ pb} \pm 0.5\%$ (error statistical) is obtained using EEG, the $O(\alpha^3) e^+e^- \rightarrow e^+e^-(\gamma)$ Monte Carlo program from Berends and Kleiss²³ and a full detector simulation. We obtain an integrated luminosity $\mathcal{L} = 21.51 \pm 0.19 \pm 0.26 \text{ pb}^{-1}$. Table III summarizes the error contributions to the LAC luminosity value.

4.2 End Cap Calorimeter Bhabha Luminosity Measurement

The second integrated luminosity measurement uses Bhabha events going into the ECC in the region $0.74 < |\cos \theta| < 0.86$. This region is used because it ensures complete trigger efficiency and allows charged particle tracking to be performed with the main drift chamber.

Because the ECC was not fully operational at the start of the run, an ECC luminosity measurement is not available for approximately 27% of the data sample.

We apply the following cuts to select Bhabha events:

1. There must be at least two showers with at least 6 GeV of energy ($\approx 0.4 \cdot E_{beam}$) in the ECC. If there are more than two, the two with the smallest acollinearity angle are used.
2. The tracks associated with each of the two showers must both be in the angular region $0.74 < |\cos \theta| < 0.86$ and one track must satisfy $0.763 < |\cos \theta| < 0.842$. θ is measured using the DC if available; otherwise the ECC shower position is used; (98.5% of Bhabha tracks are reconstructed by the DC in this angular region.)
3. If there is no DC track associated with an ECC shower, there must be at least 25 DC wire hits (out of 72 layers) within ± 15 degrees in ϕ of the shower and no DC track in this ϕ region unassociated with the ECC shower.

In Cuts 2 and 3, a drift chamber track is associated with an ECC shower if it intersects the front face of the ECC within 5 cm of the position of the shower (corresponding to a difference in angular position of $\simeq 2$ degrees). This means that radiative Bhabha events in which a high energy photon is close to an electron are counted as Bhabha events.

The tighter cut in θ placed on one track in Cut 2 reduces the sensitivity of the analysis to small errors in the Monte Carlo simulation of the Bhabha acollinearity distribution and the angular resolution of the detector. Monte Carlo event generators tend to produce too many events at zero acollinearity and too few events at small acollinearity angles, but simulate the larger angles very well. A precise cut is chosen so the acollinearity of the event must be at least two degrees for the second track to fail the gross cut. Since 90% of events have acollinearities less than two degrees, the gross cut affects only a very small fraction of events.

A total of 17178 events pass these cuts. For the same set of runs, ‘9682 Bhabha’ events are selected by the wide-angle Bhabha analysis (Section 4.1).

The analysis efficiency has been calculated with the Bhabha generator EEG from Berends and Kleiss, which includes a detailed detector simulation. We find $\epsilon_b \sigma_b = 1.098 \pm 0.004$ nb.

The trigger efficiency is measured as a function of energy deposited in the ECC using non-Bhabha events that satisfy the charged particle trigger. The overall trigger inefficiency for Bhabha events is less than 0.1%.

The background from the process $e^+e^- \rightarrow \gamma\gamma$ is estimated by Monte Carlo simulation to be fewer than five events. This rate is much lower than that of the wide-angle analysis because both tracks are required to be charged. Events from the process $e^+e^- \rightarrow e^+e^-e^+e^-$ are distinctive in that both tracks tend to have relatively

low energy compared to beam energy. The scatter plot of one shower energy versus the other indicates that there are fewer than ten such events in the data sample. This observation is in good agreement with the Monte Carlo prediction of six events from this source. The Monte Carlo prediction for the background from τ production is fewer than five events. Since all of these backgrounds are small, no correction is made to the data.

The primary sources of systematic error are summarized in Table IV. The largest individual contribution is in the definition of the precise θ cut. Varying the precise region from 0.763-0.842 to 0.780-0.827 (i.e., from 2 degrees smaller than the gross region to 3.5 degrees smaller) increases the integrated luminosity measured with the EEG Monte Carlo by 2.0%. The other errors listed in the table are the observed variations in integrated luminosity that result when the parameter used to associate DC tracks with ECC showers is varied from 5 cm to 20 cm, or the energy cut is varied between 4 GeV and 8 GeV, or an acollinearity cut is made at 10 degrees.

The integrated luminosity value obtained from the ECC for the data subsample when the ECC system was on is $15.64 \pm 0.12 \pm 0.32 \text{ pb}^{-1}$.

4.3 Small-Angle Tagger Bhabha Luminosity Measurement

The small-angle tagging system was built to measure the luminosity using small-angle Bhabha scattering. It consists of two pairs of back-to-back modules at 2 degrees to the beam axis, each module having three position-defining scintillation counters and a shower counter. Since this system has not been described in any previous publication, a more complete hardware description is given in Appendix A.

Criteria to select Bhabha tracks are based on a coincidence between a small defining scintillation counter in one module, and a larger scintillation counter in the opposite module. This way, one allows for apparent acollinearities due to beam spot

size and motion, misalignments, and radiative effects. The associated shower counters are each required to have more than 65% of the beam energy. Hits also are required in the other two scintillation counters in the module, in which the defining counter was hit in order to reduce backgrounds due to random hits and splash-back (where a Bhabha track missed the defining counter but debris from the shower hit it).

The Bhabha cross section for this system is about 400 times the total hadronic cross section, so statistical errors are negligible. The systematic errors are summarized in Table V. The misalignment correction comes from using precision survey values of the counter positions in place of the design positions. The error includes the effect of beam spot variations. A limit on the error due to the shower energy cut is obtained by changing the threshold in the Monte Carlo by an amount equal to the shower counter energy resolution. Scattering and interactions in the beampipe are modeled with a Monte Carlo using the EGS program.²⁴ Limits on the probability of a position-delivering scintillation counter intercepting a back-scattered photon can be derived from the data by looking at events where the defining scintillation counter is hit but the large scintillation counter shadowing is not. The result is in reasonable agreement with a calculation of the effect using the EGS program. The effect of random hits is calculated using an event mixing technique, and checked by a calculation using the raw rate in each counter. Random hits are only significant in making a Bhabha track that missed the defining scintillation counter appear to hit it. A limit is placed on scintillation counter inefficiencies by looking at the pulse height spectra from those counters.

The luminosity determined by the small-angle tagging system is $21.6 \pm 0.5 \text{ pb}^{-1}$.

4.4 Combined Integrated Luminosity

Table VI summarizes the integrated luminosity values measured with the three detector subsystems. The first column shows the values for the subsample where ECC data are available. The measurements by the different subsystems agree. The second column shows the integrated luminosity values for the whole data sample as measured with LAC and SAT. Except for missing higher-order QED corrections in the Monte Carlo simulation program all three measurements are largely independent of each other. The weighted average luminosity is $\mathcal{L} = 21.52 \pm 0.27 \text{ pb}^{-1}$.

5. HIGHER-ORDER QED RADIATIVE CORRECTIONS

Previous QED Monte Carlo programs, which are used to determine the detection efficiencies for hadronic and Bhabha events, have used cross section calculations only to the order $O(\alpha^3)$. Uncertainties due to missing higher-order QED corrections have been generally ignored. However, for example, the $O(\alpha^3)$ correction of the accepted* cross section for the hadrons with our cuts is about 19%. It is therefore not obvious why higher than $O(\alpha^3)$ corrections are negligible.

Previously, only the MAC collaboration has made an attempt to determine the effect on R due to higher-order QED corrections.²⁵ They used a renormalization group scheme proposed by Tsai²⁶ to calculate the cross section change for Bhabha and hadronic events. For the Bhabha events they also used the Weizsacker-Williams method to simulate the acollinearity distribution according to higher-order in QED. As a result they find that their measured R value has to be corrected by $(-1.1 \pm 1.1)\%$.

Recently the cross section for the process $e^+e^- \rightarrow \mu^+\mu^-$ has been calculated to the order $O(\alpha^4)$ including “exponentiation”²⁷ and implemented in the event generator MMGE²⁸ (see Appendix B.I). “Exponentiation” is a method to include initial state

radiation to all orders in the cross section. It also allows the artificial photon cut-off parameter, $k_0 = E_0/E_{beam}$, which separates the soft from the hard initial state radiation at the energy E_0 , to be reduced from 0.01 to an arbitrarily small value. It should be noted, however, that while MMGE calculates the initial state radiation process to all orders, the total radiated energy is given to only one effective photon.

We have implemented MMGE into the LUND Version 6.3 parton shower and hadronization Monte Carlo in order to determine the change of the hadronic acceptance due to the higher-order QED correction. For that purpose we also had to implement the vacuum polarization term which is missing in MMGE. We used the same vacuum polarization as in the $O(\alpha^3)$ generator. We find that the hadronic acceptance $\epsilon_h(1 + \delta_h)$ drops by $(0.3 \pm 0.3)\%$ compared to the $O(\alpha^3)$ LUND Monte Carlo. The 0.3% error is due to the limited Monte Carlo event statistics.

For the Bhabha cross section, the $O(\alpha^4)$ calculation has not yet been done. However, the “exponentiation” can be implemented into EEG analogously to the exponentiation of the process $e^+e^- \rightarrow \mu^+\mu^-$ (see Appendix B.2). As in MMGE, the exponentiation takes initial state radiation contributions to all orders into account and allows the k_0 cutoff parameter to be much smaller than 0.01.

Table VII summarizes the relative changes of the accepted cross sections due to the exponentiation of the Bhabha and the hadronic event generators. The effect on R , which is proportional to the ratio of Bhabha and hadron acceptances, is listed in the last column of the table. The change of the weighted average luminosity value is shown in the last row. Combined with the shift of the hadronic part it causes R to decrease by $(0.2 \pm 0.4)\%$. We therefore estimate the uncertainty of our R value due to missing higher-order radiative QED corrections to be 0.4%.

6. RESULTS

From Eq. (5) we find the value for R to be:

$$\begin{aligned}
 \mathbf{R} &= \frac{N_h - N_{BG}}{\epsilon_h(1 + \delta_h) \sigma_\mu^0 \mathcal{L}} \\
 &= 3.92 \pm 0.05 \text{ (statistical)} \pm 0.09 \text{ (systematic)}
 \end{aligned}
 \tag{6}$$

Table VIII summarizes the error contributions to \mathbf{R} and includes an entry estimating the systematic uncertainty due to missing higher-order QED corrections in the Monte Carlo event generators. The dominant sources of error, however, are the fiducial and energy cuts applied in the hadron event selection, the determination of the integrated luminosity, and the statistical error.

The value of \mathbf{R} is in agreement with other \mathbf{R} measurements done at similar energies as listed in Table IX. These values agree well with the theory expressed in Eq. (1), where five pointlike interacting quarks with spin 1/2, fractional electric charge, and three color degrees of freedom are assumed.

The last column in Table IX lists the corrections to \mathbf{R} due to higher than $O(\alpha^3)$ QED processes. Only MAC and our measurement so far estimate this effect. MAC finds a correction of $(-1.1 \pm 1.1)\%$ using a somewhat more analytical approach; for our experiment we find an averaged correction of $-0.2 \pm 0.4\%$ using a higher-order QED cross-section calculation in the Monte Carlo simulation. It should be emphasized that the effects of higher-order QED corrections are dependant on the detector acceptance. For example, the higher-order radiative corrections of the integrated luminosity values vary by up to 1.4% depending on what angular region of the detector the Bhabha events are counted in (Table VII).

One can extract the strong coupling constant α_s from the \mathbf{R} value using Eq. (1) with the expansion coefficients C_2 and C_3 calculated in the MS renormalization

scheme. For $\sin^2 \theta_W = 0.23$, we obtain $\alpha_s(29^2 \text{ GeV}^2) = 0.150_{-0.076}^{+0.072}$ in second-order QCD.

A higher precision for α_s is obtained by fitting Eq. (1) through many R values from different experiments at different energies. Figure 3 shows such a fit with all published R values taken between 7 and 57 GeV.^{8,9} For the best fit, the authors find $\alpha_s(34^2 \text{ GeV}^2) = 0.158 \pm 0.020$ in second-order QCD. This value is in good agreement with our measurement.

ACKNOWLEDGMENTS

This work was supported in part by Department of Energy contracts DE-AC03-76SF00515 (SLAC), DE-AC03-81ER40050 (CIT), DE-AM03-76SF00010 (UCSC), DE-AC02-86ER40253 (Colorado), DE-AC03-83ER40103 (Hawaii), DE-AC02-84ER40125 (Indiana), DE-AC03-76SF00098 (LBL), and DE-AC02-84ER40125 (Michigan), and by the National Science Foundation (Johns Hopkins).

APPENDIX A

THE SMALL ANGLE TAGGING SYSTEM

A luminosity monitor called the Small Angle Tagging system was constructed for the 1985/1986 run of the MARK II detector at PEP, since the previous Small Angle Tagger (SAT) did not fit in the upgraded MARK II detector. Figure 3 shows the set-up of the SAT. Each of four rectangular modules consisted of three track-defining scintillation counters and one shower counter. Modules were placed to the right and left of the beampipe at each end of the MARK II detector, slanted at 40 mrad in order to point back to the interaction point. The shower counter was built with 19 layers of 1.1-cm-thick scintillator interleaved with 1/4-inch-thick lead sheets, constituting 20 radiation lengths. The energy resolution for Bhabha electrons was 7% at 14.5 GeV. The positions and dimensions of the counters are given in Table X. The section of the aluminum beampipe between the modules and the interaction point was conically formed at an 11 degree angle from the beam direction, and presented 0.1 radiation* length of material about 75 cm in front of the modules.

The output of each counter was connected to a discriminator for triggering purposes, to an ADC for offline threshold analysis, and to a TDC to differentiate between beam-spray hitting from the back of the module and particles passing through the interaction point. The electronics included a circuit to mix hits from one beam-crossover with hits from the next to get an estimate of random backgrounds.

APPENDIX B

RADIATIVE CORRECTIONS

B.1 MMGE

The MMGE program is the updated version by Alexander et al.²⁸ of the widely used p-pair generator from Berends, Kleiss, and Jadach.¹⁹ This update includes the higher-order initial state radiative corrections from Berends, Burgers, and van Neerven.^{27,29} We discuss the exponentiation of this generator in some detail since this has been duplicated as closely as possible in the Bhabha generator (EEG) discussed in Appendix B.21.

In first-order the total cross section can be written as:

$$\sigma_1(s) = \sigma_0(s) (1 + \delta_1^v + \beta \ell_n k_0) + \int_{k_0}^{k_{\text{mat}}} \beta \left(\frac{1 + (1-k)^2}{2k} \right) \sigma_0(s') dk \quad , \quad (7)$$

while in second-order this is modified to²⁸:

$$\begin{aligned} \sigma_2(s) = & \sigma_0(s) (1 + \delta_1^v + \delta_2^v + \beta \ell_n k_0 + \delta_1^v \beta \ell_n k_0 + \frac{1}{2} \beta^2 \ell_n^2 k_0) \\ & + \int_{k_0}^{k_{\text{max}}} \sigma_0(s') \left[\beta \left(\frac{1 + (1-k)^2}{2k} \right) (1 + \delta_1^v + \beta \ell_n k) \right. \\ & \left. + \left(\frac{\alpha}{\pi} \right)^2 \left\{ \left(\frac{1 + (1-k)^2}{k} \right) A(k) + (2-k) B(k) + (1-k) C(k) \right\} \right] dk \quad , \end{aligned} \quad (8)$$

Here $s(s')$ = center-of-mass energy before (after) energy loss from initial state radiation and

$$\beta = \frac{2\alpha}{\pi} \left(\ell_n \left(\frac{s}{m_e^2} \right) - 1 \right) \quad , \quad (9)$$

$$k = 1 - \frac{s'}{s} \quad , \quad (10)$$

$$\delta_1^v = \frac{\alpha}{\pi} \left[\frac{3}{2} \ln \left(\frac{s}{m_e^2} \right) - 2 + \frac{\pi^2}{3} \right] \quad . \quad (11)$$

The expressions for $\mathbf{A}(\mathbf{k})$, $B(k)$, $C(k)$ and δ_2^v have been given in Ref. 29.

Note that in first-order the energy loss parameter k is just the fractional photon energy E_γ/E_{beam} . In higher-order, when the energy loss is distributed over more photons, these latter have an invariant mass ($M_{\gamma\gamma}$) and the relation between ΣE_γ and k becomes: $k \equiv 1 - s'/s = \Sigma E_\gamma/E_{beam} - M_{\gamma\gamma}^2/s$. Since $M_{\gamma\gamma}^2/s$ is usually small, the difference between k and the total radiated fractional energy $\Sigma E_\gamma/E_{beam}$ becomes also small.

The cross sections in Eqs. (7) and (8) have been split into two parts. The first part is the part with only soft photons, so $a(s) = \sigma(s')$; the second part includes hard photon radiation, in which case $\sigma(s') \neq \sigma(s)$, so one has to convolute the energy loss spectrum with $\sigma(s')$, as is done by the expressions below the integrals. The separation between the soft and hard parts of the spectrum is defined by k_0 . For $k_0 \rightarrow 0$ the soft part goes to $-\infty$, while the hard part goes to $+\infty$. As long as k_0 is small, the sum of the two parts is independent of the choice of k_0 , as can be easily seen from Eq. (7): if one assumes $\sigma_0(s') = \sigma_0(s)s/s'$, the integral of the hard part yields:

$$\begin{aligned} \sigma_{hard} &= \beta \sigma_0 \left[\ln k_{max} - \ln k_0 - \frac{1}{2} \ln(1 - k_{max}) \right. \\ &\quad \left. + \frac{1}{2} \ln(1 - k_0) - \frac{1}{2} k_{max} + \frac{1}{2} k_0 \right] \quad (12) \\ &\approx \beta \sigma_0 \left[-\ln k_0 - \frac{1}{2} \ln(1 - k_{max}) - \frac{1}{2} k_{max} \right] \end{aligned}$$

In the last approximation we assumed $\ln(1 - k_0) \sim 0$; then

$$\begin{aligned}\sigma_{tot} &= \sigma_{soft} + \sigma_{hard} \\ &= \sigma_0(s) \left[1 + \delta_1^v - \frac{1}{2} \beta \ln(1 - k_{max}) - \frac{1}{2} k_{max} \right] \end{aligned} \quad (13)$$

is independent of k_0 .

It can be shown²⁹ that the leading terms of the real photon emission always lead to terms $(1/n!) \beta^n \ln^n \mathbf{k}$, so summing the leading logs to all orders implies “exponentiating” the cross section, which yields:

$$\sigma_{soft}^{exp}(s) = \sigma_0(s) (1 + \delta_1^v + \delta_2^v + \dots) k^\beta, \quad (14)$$

since

$$k^\beta = \exp\{\beta \ln k\} = 1 + \beta \ln k + \frac{1}{2!} \beta^2 \ln^2 k + \dots \quad (15)$$

This expression clearly reproduces the soft parts of the first- and second-order cross sections [Eqs. (7) and (8)], if the higher-order terms are dropped in the expansion.

For the virtual corrections no such simple formulae exist. Therefore they have to be calculated, a difficult task already in second-order. Fortunately the second-order-vertex correction is already small, so one may hope that the higher orders are small too. For example, at $\sqrt{s} = 29$ GeV, $\delta_1^v = 0.08$ and $\delta_2^v = -0.005$.

If one neglects the small terms proportional to $\mathbf{A}(\mathbf{k})$, $\mathbf{B}(\mathbf{k})$ and $\mathbf{C}(\mathbf{k})$ in Eq. (8), one sees that the hard part in second-order contains the factor $(1 + \delta_1^v + \beta \ln \mathbf{k})$ which can be replaced again by the exponentiated version $(1 + \delta_1^v + \dots) k^\beta$ [see Eq. (15)], so one finds:

$$\sigma_1^{exp}(s) = \int_0^{k_{max}} \beta \left(\frac{1}{k} - 1 + \frac{k}{2} \right) (\mathbf{1} + \delta_1) k^\beta \sigma_0(s) d\mathbf{k} \quad (16)$$

Note that the factor k^β regularizes the infinities (if $\mathbf{k} \rightarrow 0$ so the integral for $\mathbf{k} = \mathbf{0}$ is well behaved and one does not have to split the cross section in a hard and soft part anymore), but integrates from 0 to the kinematic limit. One can regulate the divergencies in the second-order cross section too, by exponentiating the soft part:

$$\sigma_2^{exp}(s) = \int_0^{k_{max}} \sigma_0(s') \left[a \left(\frac{1}{k} \right) (1 + \delta_1^v + \delta_2^v) k^\beta \right] d\mathbf{k} + \sigma_{2H} \quad , \quad (17)$$

where σ_{2H} contains the finite part of the cross section (everything except the $1/k$ pole).

Note that in the first-order exponentiated cross section [Eq. (16)] we have exponentiated the finite part ($-1 + \mathbf{k}/2$ term) too, while in second-order the finite part is treated exactly. Exponentiating the finite part of the first-order cross section is usually not done,²⁸ but its justification stems from the fact that in second-order this finite part is multiplied by $1 + \delta_1^v + \beta \ln k$ [see Eq. (8)] and, secondly, that σ_1^{exp} is numerically then practically identical to σ_2^{exp} . Thus, a very simple procedure for exponentiating a first-order Monte Carlo is: weight the hard part of the cross section with the factor $(1 + \delta_1^v)k^\beta$. This works perfectly in the case of p-pairs, and is probably the best guess in case of Bhabha scattering, for which no exact second-order calculation exists.

B.2 EEG

The origin of EEG is the widely used Bhabha generator from Berends and Kleiss.²³ It uses $O(\alpha^3)$ calculations for Bhabha scattering; i.e., at most one photon is allowed from initial or final state radiation. We estimate higher-order contributions by adding exponentiation to this Monte Carlo. Since exponentiation procedures are not unique, the exponentiation procedure which “works best” for p-pairs has been chosen; i.e., the procedure which gives results closest to the exact second-order calculation. As mentioned in describing the exponentiation of the p-pair generator, this corresponds

to weighting each radiative event with a factor $(1 + \delta)k^\beta$. For Bhabha scattering, final state radiation is important, in which case β should be defined as $\beta_i + \beta_f + 2\beta_{int}$, where $\beta_i = \beta_f$ equals β , as defined by Eq. (9), and Ref. 31,

$$P_{int} = \frac{4\alpha}{\pi} \ln \operatorname{tg} \frac{\theta}{2} \quad , \quad (18)$$

where θ is the polar scattering angle.

REFERENCES

1. B. Esposito et al., *Nuovo Cimento Lett.* **19** (1977) 21;
C. Bacci et al., *Phys. Lett.* **86B** (1979) 234.
2. P. A. Rapidis et al., *Phys. Rev. Lett.* **39** (1977) 526; and Ph.D. thesis, SLAC-Report-220 (1977).
3. CLEO Coll: R. Giles et al., *Phys. Rev.* **D29** (1984) 1285;
CUSB Coll: E. Rice et al., *Phys. Rev. Lett.* **48** (1982) 906.
4. DASP2 Coll: H. Albrecht et al., *Phys. Lett.* **116B** (1982) 383;
DESY-Hamburg-Heidelberg-MPI Munich Coll:
P. Bock et al., *Z. Physik* **C6** (1980) 125;
LENA Coll: B. Niczyporuk et al., *Z. Physik* **C15** (1982) 299;
PLUTO Coll: L. Criegee, G. Knies, *Phys. Rep.* **83** (1982) 153.
5. HRS Coll: D. Bender et al., *Phys. Rev.* **D31** (1985) 1;
MAC Coll: E. Fernandez et al., *Phys. Rev.* **D31** (1985) 1537.
6. JADE Coll: W. Bartel et al., *Phys. Lett.* **129B** (1983) 145; *ibid.*, **160B** (1985) 337;
B. Naroska, *Phys. Rep.* **148** (1987) 67;
MARK J Coll: B. Adeva et al., *Phys. Rev.* **D34** (1986) 681;
MARK J Coll: B. Adeva et al., *Phys. Rep.* **109** (1984) 131;
D. Linnhöfer, Ph.D. thesis, Aachen (1986);
PLUTO Coll: L. Criegee, G. Knies, *Phys. Rep.* **83** (1982) 153;
PLUTO Coll: C. Berger et al., *Phys. Lett.* **91B** (1980) 148;
TASS0 Coll: R. Brandelik et al., *Phys. Lett.* **113B** (1982) 499;
M. Althoff et al., *Phys. Lett.* **138B** (1984) 441 and private communication.

7. VENUS Coll: H. Yoshida et al., *Phys. Lett.* **198B** (1987) 570;
 AMY Coll: H. Sagawa et al., *Phys. Rev. Lett.* **60** (1988) 93;
 T. Mori et al., submitted to *Phys. Lett.*;
 TOPAZ Coll: I. Adachi et al., *Phys. Rev. Lett.* **60** (1988) 97;
 AMY Coll: T. Kumita et al., submitted to *Phys. Rev. D*.
8. CELLO Coll: H. J. Behrend et al., *Phys. Lett.* **183B** (1987) 400.
9. G. d'Agostini, W. de Boer, and G. Grindhammer, *Phys. Lett.* **229B** (1989) 160.
10. J. Ellis and M. K. Gaillard, "Physics with Very High Energy e^+e^- Colliding Beams," CERN Report 76-18 (1976);
 J. Jersac, E. Laermann, and P. M. Zerwas, *Phys. Lett.* **98B** (1981) 363.
11. M. Dine and J. Sapirstein, *Phys. Rev. Lett.* **43** (1979) 668;
 K. G. Chetyrkin et al., *Phys. Lett.* **85B** (1979) 277;
 W. Celmaster and R. J. Gonsalves, *Phys. Rev. Lett.* **44** (1980) 560.
12. S. G. Gorishny, A. L. Kataev and S. A. Larin, *Phys. Lett.* **212B (1988) 238**.
13. SLAC Coll: "Proposal for the MARK II at SLC," SLAC-PUB-3561 (1985).
14. W. T. Ford et al., *Nucl. Instrum. Methods* **A255** (1987) 486.
15. G. Hanson, *Nucl. Instrum. Methods* **A252** (1986) 343.
16. W. Farr et al., *Nucl. Instrum. Methods* **156** (1978) 283.
17. G. S. Abrams, *IEEE Trans. Nucl. Sci.* **27** (1980) 59.
18. M. Bengtsson and T. Sjöstrand, *Comp. Phys. Comm.* **43** (1987) 367.
19. F. A. Berends, R. Kleiss, and S. Jadach, *Nucl. Phys.* B202 (1982) 63; and
Comp. Phys. Comm. **29** (1983) 185.
20. M. Bengtsson and T. Sjöstrand, *Phys. Lett.* **185B** (1987) 435.
21. MARK II Coil: A. Petersen et al., *Phys. Rev.* **D37** (1988) 1.

22. F. A. Berends, P. H. Daverveldt, and R. Kleiss, *Nucl. Phys.* **B253** (1985) 441;
Comp. Phys. Corn. **40** (1986) 285.
23. F. A. Berends and R. Kleiss, *Nucl. Phys.* **B228** (1983) 537.
- 24.** W. R. Nelson et al., "The EGS4 Code System," SLAC Report 265 (1985).
25. MAC Coll: E. Fernandez et al., *Phys. Rev.* **D31** (1985) 1537.
26. Y. S. Tsai, *Proc. 1st Asia-Pacific Physics Conf., Vol. 2*, Singapore, 1983,
pp. 1289-1339; SLAC-PUB-3129 (1983).
27. F. A. Berends, G. J. H. Burgers, W. L. van Neerven, *Phys. Lett.* **185B** (1987)
395.
28. J. P. Alexander, G. Bonvicini, P. S. Drell, and R. Frey; *Phys. Rev.* **D37** (1988)
56.
29. F. A. Berends, G. J. H. Burgers, and W. L. van Neerven, *Nucl. Phys.* **B297**
(1988) 429.
30. D. R. Yennie, S. C. Frautschi, H. Suura, *Ann. of Phys.* **13** (1961) 379.
31. M. Greco, *Riv. Nuovo Cim.* **5** (1988) 1; and *Phys. Lett.* **177B** (1986) 97.
Also see Berends and Komen, *Nucl. Phys.* **B115** (1976) 114.
32. J. D. Patrick, Ph.D. thesis, LBL-14585 (1982), unpublished.

TABLE CAPTIONS

1. Sequence of the hadron selection cuts and the resulting efficiencies ϵ_h as determined from Monte Carlo simulation (see text).
2. Summary of background contributions, systematic error estimations, and the final hadronic sample.
3. Summary of the systematic errors for the luminosity determination with wide-angle Bhabhas.
4. Sources of systematic errors in the ECC luminosity measurement.
5. Estimated systematic corrections and errors of luminosity measurement using the Small Angle Tagging system.
6. Comparison of ECC, LAC and SAT integrated luminosity values for the complete data sample and the subsample where ECC data are available. For determining the weighted average luminosity value, the data of the ECC subsample are included.
7. Relative changes of the Bhabha and hadron event acceptances due to the exponentiation of the cross sections in the Bhabha and hadron events generators. The variations for the Bhabha events are shown for the three different angular ranges of the LAC, ECC and SAT. The last row shows the weighted average values. The last column shows the resulting change in R .
8. Summary of the systematic errors for R .
9. Comparison of the R measurement values at PEP and PETRA as taken from the literature. The last column lists the estimated shifts due to missing higher than $O(\alpha^3)$ QED corrections in the Monte Carlo generators if available. The

MARK II/PEP measurement was done with data taken prior to the detector upgrade.

10. Small Angle Tagging system counter locations and sizes (in cm).

TABLE I

Cut	Events	ϵ_h	Events/q.
$N_{ch} > 4$	16153	0.811	19917
$E_{ch} > 0.26E_{cm}$	8113	0.680	11931
$E_{vis} > 0.4E_{cm}$	7649	0.644	11877
$p_T, \Sigma p_{z_i} < 10 \text{ GeV}$	7567	0.640	11823
$ \Sigma q_i < 5$	7526	0.637	11815
$ Z_v < 6 \text{ cm}$	7521 ± 87	0.637 ± 0.003	11807 ± 145

TABLE II

	Value	Statistical Error	Systematic Error
Events	7521	1.2%	
Background:			—
$\tau^+\tau^-$	0.9%		0.4%
Beam gas	<0.1%	—	—
Two photon	1.0%	—	0.4%
Bhabha	0.5%	—	0.3%
Subtotal:	2.4%		0.6%
Track Cuts:			
$ \cos(\theta_{track}) $	—	—	1.1%
$ Z_{tr} $	—	—	0.2%
Subtotal:		—	1.1%
Event Cuts:			
$N_{ch} > 4$	—	—	0.6%
$E_{ch} > 0.26 E_{cm}$	—	—	0.9%
$E_{vis} > 0.4 E_{cm}$		—	0.4%
$ \Sigma p_{x,y,z} < 10 \text{ GeV}$	—	—	0.2%
Subtotal:		—	1.2%
Final N_h	7340	$\pm 1.2\%$	$\pm 1.7\%$

TABLE III

	Value	Statistical Error	Systematic Error
Events	13295	0.9%	—
Background:			
$e^+e^- \rightarrow \gamma\gamma$	1.1 %	—	0.5 %
$e^+e^- \rightarrow \tau^+\tau^-$	<0.1%	—	—
$e^+e^- \rightarrow e^+e^-e^+e^-$	<0.1%	—	—
N_{Bhabha} :	13149	0.9%	—
Event Cuts:			
\$-crack cut	—	—	0.3 %
Fine/gross fiducial vol	—	—	0.4 %
Cone acollinearity	—	—	0.3 %
Cone energy cut	—	—	0.8 %
ϵ_{tr}	0.998	—	0.1 %
$\epsilon_b\sigma_b$ (Monte Carlo):	611.4 pb	—	0.5%
$\mathcal{L} = N_{Bhabha}/(\epsilon_b\sigma_b) [\text{pb}^{-1}]$	21.51	$\pm 0.9\%$	$\pm 1.2\%$

TABLE IV

Source	Systematic Error EEG
Fiducial cut	2.0%
Monte Carlo statistics	0.4%
DC/ECC association	0.2%
Detector simulation	0.3%
Energy cut	0.1%
Acollinearity	0.1%
Total	2.1%

TABLE V

Source	Correction	Estimated Error
Misalignment, spot sizes	+0.8%	$\pm 1.3 \%$
Shower energy threshold		$\pm 0.6 \%$
Beampipe interactions	-1.2%	$\pm 1.2 \%$
Splashback		$- 0.8 \%$
Random noise hits		$\pm 0.8\%$
Scintillator inefficiency		+ 1.0%
Total Systematic Correction	-0.4%	$\pm 2.5\%$

TABLE VI

Detector Subsystem	Integrated Luminosity ECC Subsample [pb^{-1}]	Integrated Luminosity Total Data Sample [pb^{-1}]
LAC	$15.66 \pm 0.16 \pm 0.19$	$21.51 \pm 0.19 \pm 0.26$
ECC	$15.64 \pm 0.12 \pm 0.32$	—————
SAT	$15.74 \pm 0.01 \pm 0.39$	$21.59 \pm 0.01 \pm 0.54$
Weighted Average:		21.52 ± 0.27

TABLE VII

Relative Change:	Bhabha Events: $\Delta[\epsilon_b(1 + \delta_b)]$	Hadrons: $\Delta[\epsilon_h(1 + \delta_h)]$	$\Delta[R]$
LAC Region	$(-0.6 \pm 0.2)\%$	$(-0.3 \pm 0.3)\%$	$(-0.3 \pm 0.4)\%$
ECC Region	$(-1.1 \pm 0.2)\%$	$(-0.3 \pm 0.3)\%$	$(-0.8 \pm 0.4)\%$
SAT Region	$(0.3 \pm 0.3)\%$	$(-0.3 \pm 0.3)\%$	$(0.6 \pm 0.4)\%$
Weighted Average	$(-0.5 \pm 0.2)\%$	$(-0.3 \pm 0.3)\%$	$(-0.2 \pm 0.4)\%$

TABLE VIII

Quantity	Value	Statistical	Systematic
N_h	7340	1.2%	1.7%
$\epsilon_h(1 + \delta_h)$	0.8432		0.4%
\mathcal{L} [pb ⁻¹]	21.52		1.3%
QED correction $> O(\alpha^3)$:			0.4%
R Value	3.92	1.2%	2.2%

TABLE IX

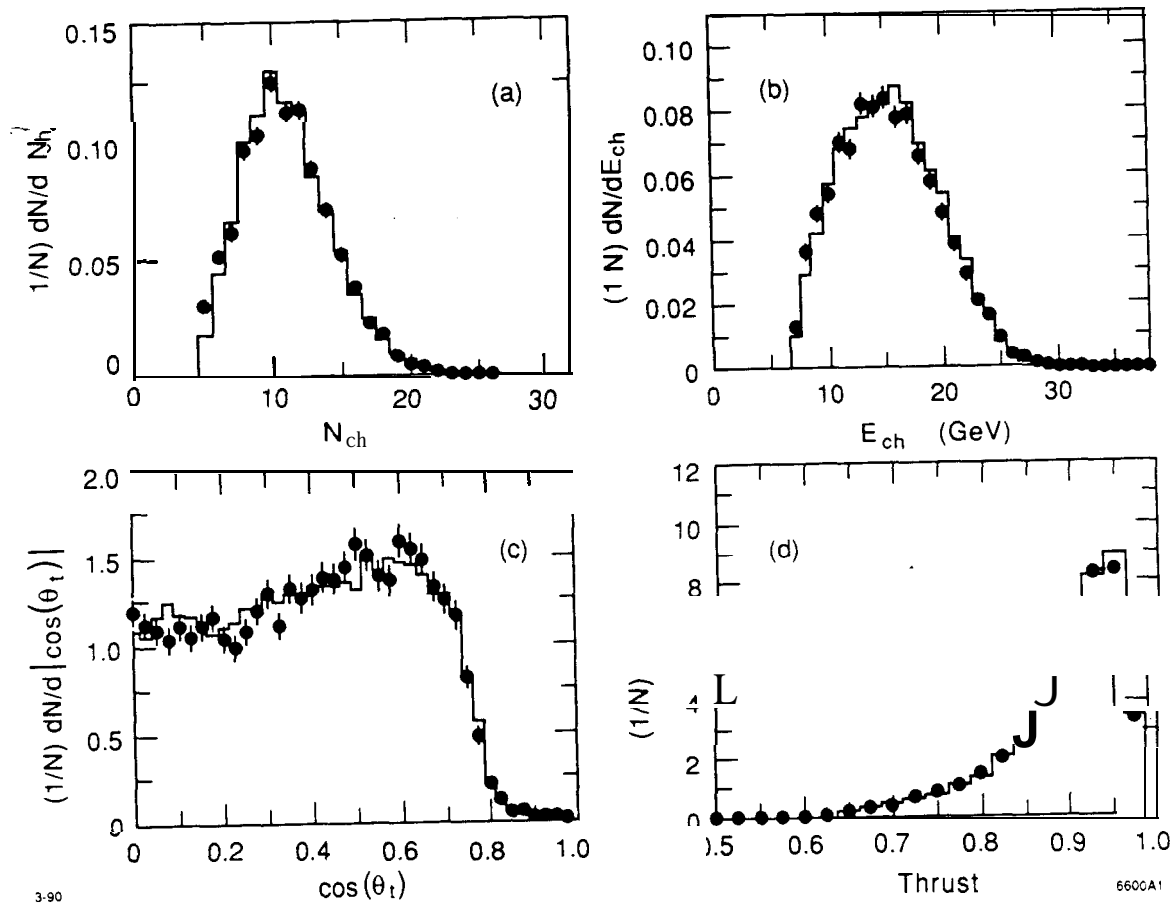
Experiment	E_{cm} [GeV]	R-Value $O(\alpha^3)$	$> O(\alpha^3)$ Corr.
This measurement	29	$3.92 \pm 0.05 \pm 0.09$	$(-0.2 \pm 0.4)\%$
CELLO ('87) ⁸	33.8	$3.74 \pm 0.10 \pm 0.10$	—
MAC ('85) ⁵	29	$4.00 \pm 0.03 \pm 0.09$	$(-1.1 \pm 1.1)\%$
HRS ('85) ⁵	29	$4.20 \pm 0.05 \pm 0.29$	
MARK J ('84) ⁶	12-42.6	$3.88 \pm 0.04 \pm 0.22$	
JADE ('83) ⁶	12-36.4	$3.97 \pm 0.05 \pm 0.10$	—
TASSO ('82) ⁶	12-36.4	$4.01 \pm 0.03 \pm 0.20$	—
MARK II/PEP ('82) ³²	29	$3.90 \pm 0.05 \pm 0.25$	
PLUTO ('80) ⁶	29.9-31.5	$3.90 \pm 0.2 \pm 0.5$	—

TABLE X

Counter	z	x at Center	Width	Height	Thickness
Defining	310.0	12.446	5.080	6.350	1.270
Large	311.6	12.510	7.620	8.890	1.270
Background suppress	329.9	13.249	5.715	6.985	0.635
Shower	331.9	13.739	13.000	15.000	

FIGURE CAPTIONS

1. Comparison of the observed data event distributions (points) with LUND 6.3 Monte Carlo events (histogram) after the selection cuts: (a) charged multiplicity, (b) charged energy, (c) cosine of thrust axis to the beam direction, and (d) thrust.
2. Variation of the number of events N_i corrected for their detection efficiency ϵ_i for varying cut parameters. This cut dependence is used to estimate the systematic error due to the cuts in the (a) charged multiplicity, (b) charged energy, (c) fiducial volume for tracks, and (d) visible energy. The error bar in each of the plots indicates the statistical error in N_i/ϵ_i .
3. A best fit of the Standard Model through the averaged measured R values between 7 and 57 GeV center-of-mass energy. The fit yields $\alpha_s(34^2 \text{ GeV}^2) = 0.158 \pm 0.020$ in second-order QCD. For more details, see Refs. 8 and 9.
4. Schematic view on the Small Angle Tagger as used for the fast luminosity measurement for the upgraded MARK II detector runs at PEP.



3-90

6600A1

Fig. 1

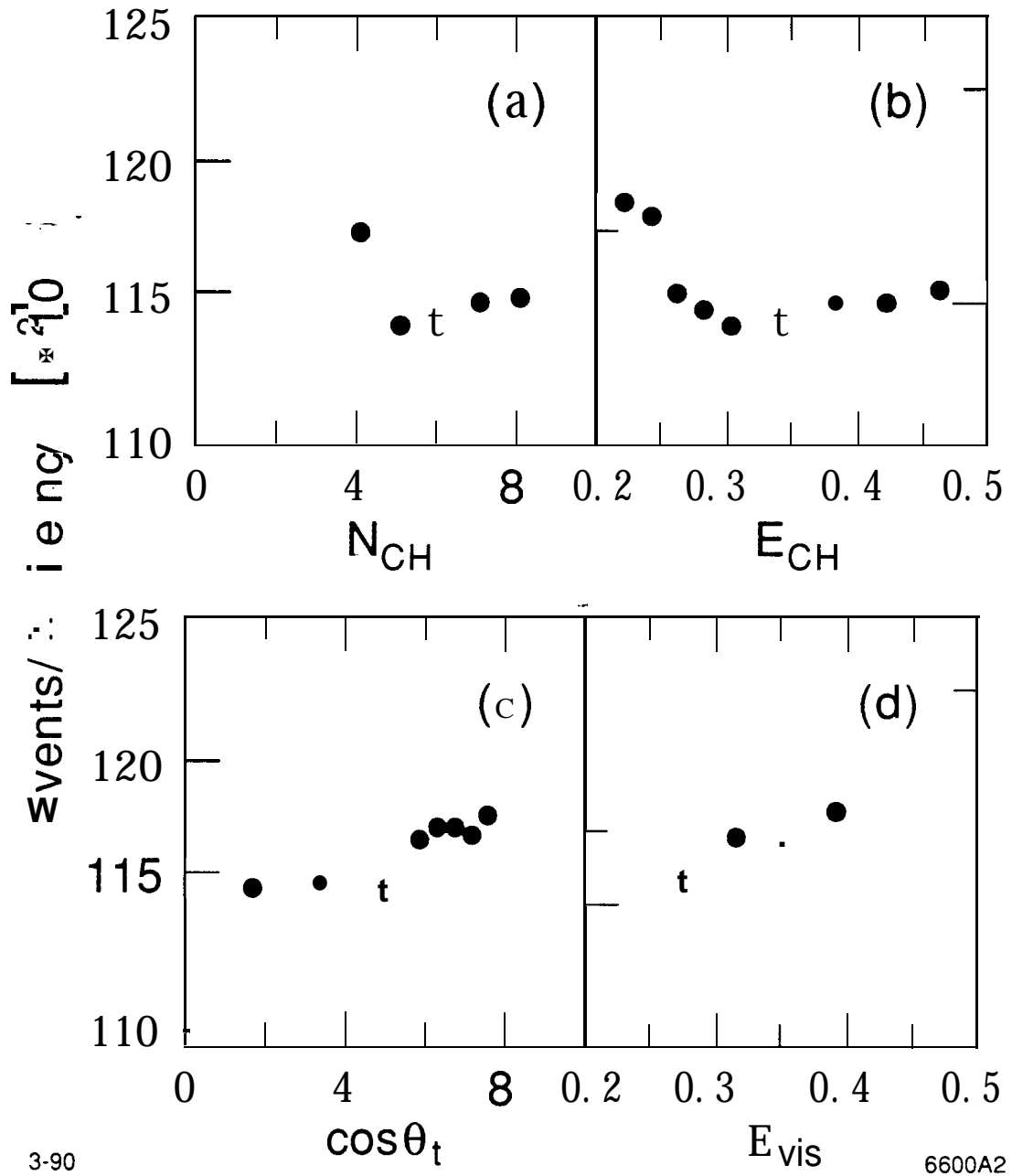


Fig. 2

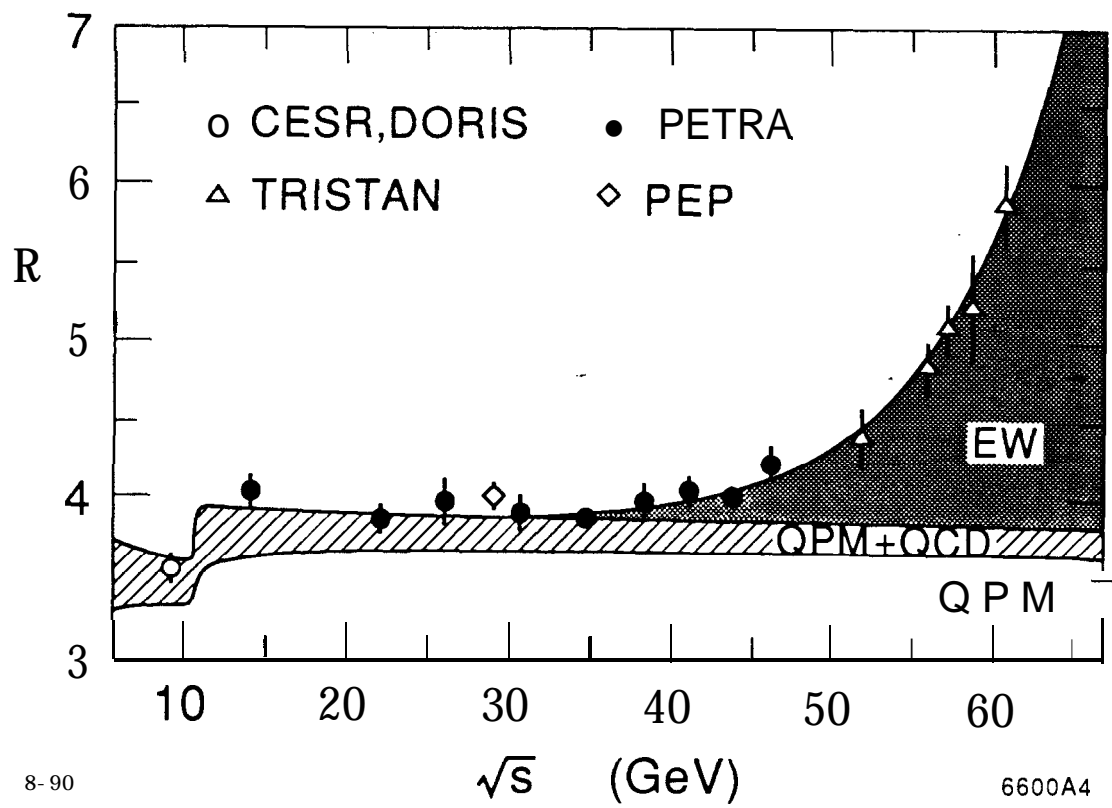


Fig. 3

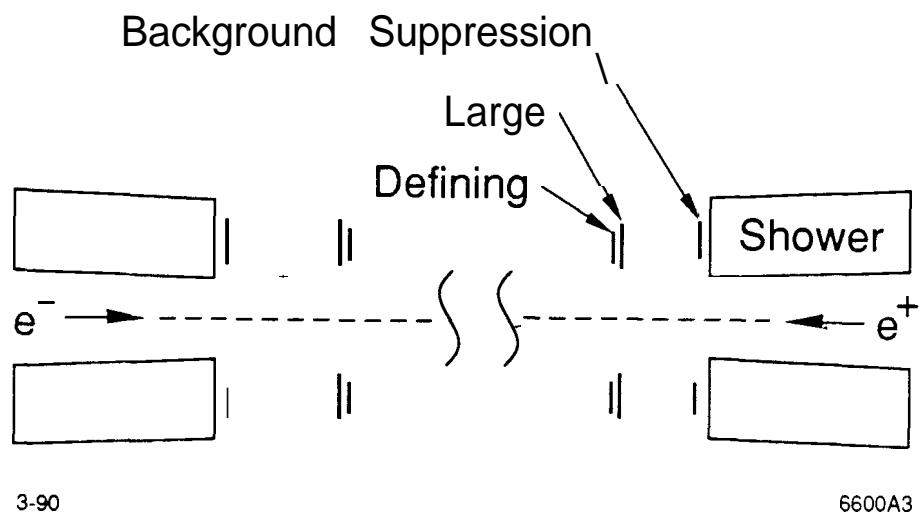


Fig. 4